Estimating local seeing at the DCT facility

Dan Blanco*
NOAO, 950 N. Cherry Ave, Tucson, AZ 85719, and
College of Optical Sciences, the University of Arizona
1630 E. University Blvd, Tucson, AZ 85721

Abstract

A thermal model of the Discovery Channel Telescope (DCT) was used to estimate the contribution of major sources of local seeing; shell seeing, dome seeing and mirror seeing. The model simulates a dynamic equilibrium over several day/night cycles taking into account the morphology of the facility, diurnal insolation and radiation to the night sky, local air temperature and humidity swings, wind and air flow through the facility, and infiltration from warm spaces within the facility. The model confirmed that the well ventilated design of the DCT facility will virtually eliminate dome seeing, but that shell seeing and mirror seeing could be major contributors to local seeing. These can be mitigated by the choice of an appropriate exterior coating, and by cooling the primary mirror.

Keywords: Dome seeing, mirror seeing, shell seeing

1. Major sources of local seeing

"Telescopes… cannot be so formed as to take away that confusion of the Rays which arises from the Tremors of the Atmosphere. The only Remedy is a most serene and quiet Air, such as may perhaps be found on the tops of the highest Mountains above the grosser Clouds." (Isaac Newton, 1730).

Selecting a good site does not in itself assure good seeing; the observatory facility itself can introduce a "confusion of Rays," or local seeing. A review of recent literature identified three major sources of local seeing:

1. Shell seeing arises when the exterior surface temperature of the dome shell differs from local ambient air temperature. A mixing layer forms at the dome slit as a layer of air heated or cooled by contact with the dome shell mixes with air both inside and outside the dome (see Figure 1). In schlerien images, shell seeing can be identified as ripples that propagate across the pupil at the local wind speed.

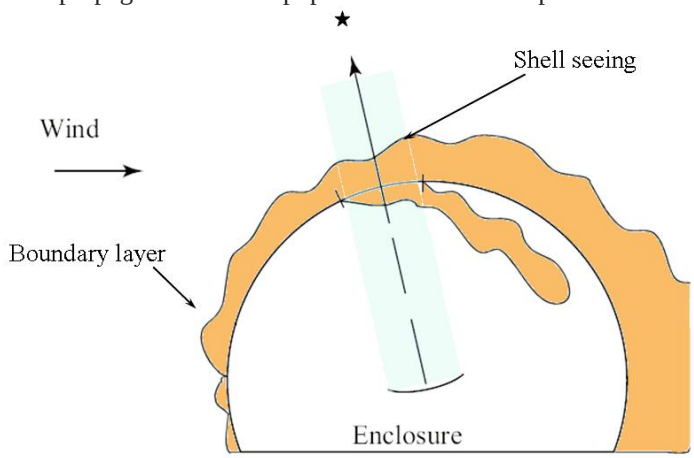

Figure 1. Shell seeing results from air heated or cooled by convection from the shell of the dome. As this air passes over the optical beam it is observed as shell seeing.

* dblanco@noao.edu

Ground-based and Airborne Telescopes II, edited by Larry M. Stepp, Roberto Gilmozzi,
Proc. of SPIE Vol. 7012, 70123V, (2008) · 0277-786X/08/$18 · doi: 10.1117/12.789649

2. Dome seeing arises from interior surfaces and structures that differ in temperature from the air inside the chamber. Heat dissipated from active equipment also contributes to dome seeing. Warm surfaces can generate plumes of warm air that pass through the optical beam. Generally cool surfaces are less troublesome, though these too can be lofted by a light breeze into the optical beam (see Figure 2). In schlerien images, dome seeing can be identified as pockets or bubbles that move slowly across the pupil.

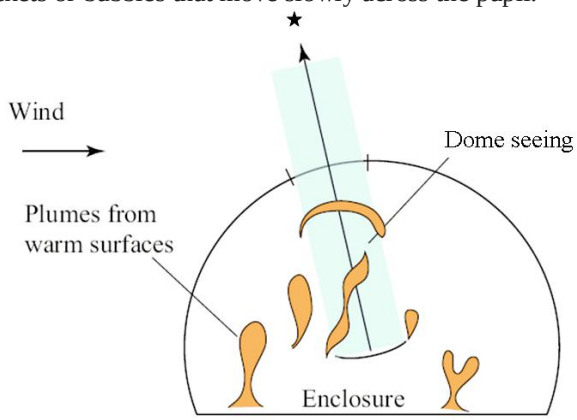

Figure 2. Warm areas of the enclosure including e.g. floor, walls, telescope or other structure generate rising plumes of warm air. As these plumes pass into the optical beam they are observed as dome seeing. Illustration adapted from Dalrymple [2004].

3. Mirror seeing arises when the primary mirror is warmer than the surrounding air. The effect is strongest in still air and decreases as the air speed over the mirror increases. Schlerien of severe mirror seeing looks like the surface of a boiling fluid.

These are not the only sources of seeing; the smaller optics, the telescope mass, the chamber floor can contribute to the local seeing if they are much warmer or cooler than the ambient air. These sources should not be neglected, but they are relatively minor contributors compared to the three dominant sources.

2. Quantifying seeing contributions

Expressions for estimating the contribution from each of these major sources can be found in the literature. An analysis by Robert Ford [1993] for the Gemini 8m telescopes developed an expression for shell seeing. Dalrymple [200] continued Ford's analysis to find a simple expression:

$$\theta_{shell} = 0.12 \cdot \Delta T_{a\text{-}s}^{\ 1.2} \qquad (1)$$

where $\mathbf{T_{a\text{-}s}}$ is the temperature difference between ambient air and the surface of the dome shell.

Rene Racine [1991] developed an expression for dome seeing based on observations at CFHT. He found good correlation between dome seeing and the temperature difference between the observing chamber and the ambient air:

$$\theta_{dome} = 0.10 \cdot \Delta T_{c\text{-}a}^{\ 1.2} \qquad (2)$$

where $\mathbf{T_{c\text{-}a}}$ is the temperature difference between the dome chamber interior and the ambient air.

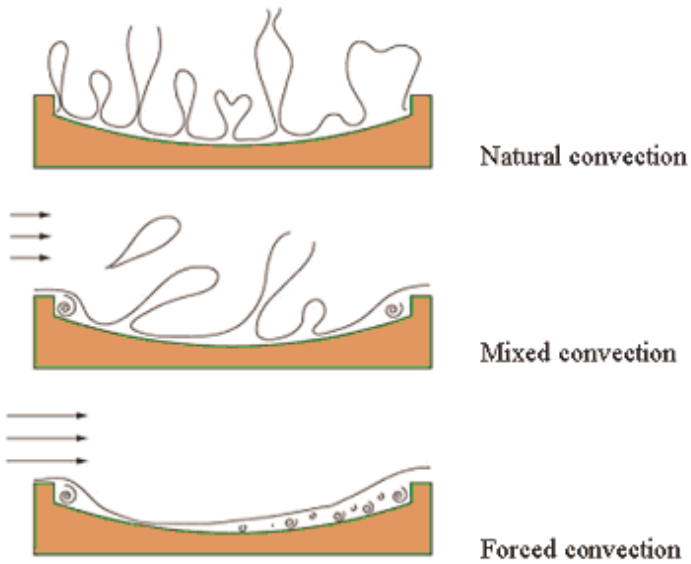

Figure 3. Mirror seeing has three regimes according to the velocity of air moving over the mirror surface. Adapted from Dalrymple [2003]

Lorenzo Zago [1995] identified three regimes for mirror seeing illustrated in Figure 3. In still air a warm mirror will develop convection cells driven by the buoyancy of the air. Each consists of a central plume of warm air surrounded by a tube of descending cooler air. The differing air temperature in the cell structure has a strong effect on seeing, but the structure is fragile; a small breeze will precipitate transition into a mixed regime. At higher wind velocities the flow pattern becomes fully forced and seeing is reduced. Zago developed expressions to quantify these effects:

In still air, $$\theta_{mirror} = 0.38 \cdot \Delta T_{c\text{-}m}^{1.2} \quad (3)$$

For mixed to forced regimes, $$\theta_{mirror} = 0.18 \cdot \Delta T_{c\text{-}m} / Fr^{0.3} \quad (4)$$

where $Fr = T_c \cdot U^2 / (\Delta T_{c\text{-}m} \cdot g \cdot L)$
g is gravitational acceleration
L is the mirror diameter
$T_{c\text{-}m}$ is the chamber air to mirror surface temperature difference
U is wind speed

A mirror that is colder than ambient tends to suppress seeing, however if the mirror is much colder than ambient it may re-introduce seeing at a lesser temperature-difference dependency than suggested by Zago. Moreover, there is a risk of condensation forming on a mirror that is much colder than ambient. A good target temperature range is ambient to two degrees below, with due attention to the dew point when operating in high relative humidity. For this study we assume that mirror seeing is nil when the mirror is below ambient:

For a mirror that is colder than ambient, $$\theta_{mirror} \approx 0 \quad (5)$$

Zago's expressions have been independently confirmed by several investigators and are generally considered reliable. For example see Blanco et al [2000]. As for shell seeing there is little doubt that expression 1 correctly describes the trend; several observatories have recoated white-painted domes with either aluminized tape or silver paint with unanimous anecdotal reports that the seeing improves as a result. However, quantitative results are not readily available so the accuracy is difficult to verify.

3. Estimating temperatures

Armed with expressions 1-5 we can estimate the local seeing based on wind speeds and temperature estimates for the facility. In particular we need to estimate:

- Ambient air temperature at the site
- The surface temperature of the dome shell
- The temperature of the air inside the observing chamber
- The temperature of the primary mirror surface
- The wind speed at the mirror surface

A computational fluid dynamic study done by TFD [2003] estimated the wind speed at various points around the facility. In order to estimate temperatures, a transient thermal model of the facility was built using the commercial thermal analysis program WinTherm® available from ThermoAnalytics, Inc. [www.ThermoAnalytics.com], a finite difference program well suited to modeling thermal transients. In the finite difference method heat transfer is expressed as rate equations that describe storage, conduction, convection, radiation, internal generation and advection to and from elements of the model. The program iterates through small time steps to numerically solve for the temperature of each element at any given time. A nice feature of the program is its extensive library of thermal properties of materials and surface coatings. In addition, the program can calculate insolation based on the global coordinates and the time of year. Initial models were run for four days to assure that dynamic equilibrium had been reached. Subsequent models cover a 48 hour period near the vernal equinox.

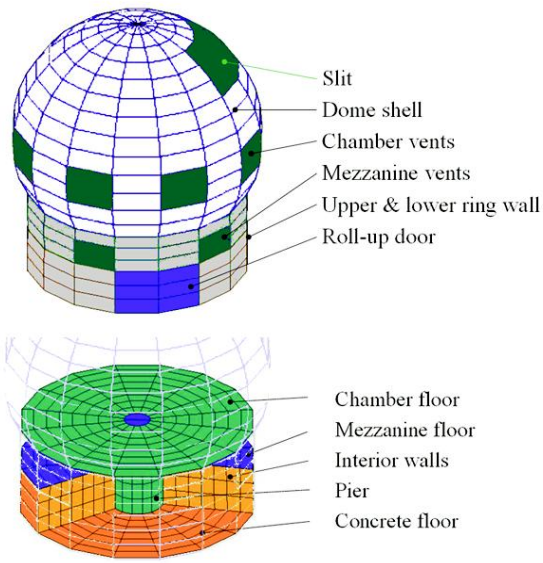

Figure 4. Exterior and interior features of the WinTherm® model. The telescope structure was modeled as a single node representing its exposed surface area and thermal capacitance.

4. Transient thermal model

The DCT facility [Terán et al, 2003] is a steel framed, metal clad building designed to equilibrate rapidly with large passive ventilation grills in the dome and mezzanine levels. The base of the facility includes heated and cooled spaces; a control room, an instrument workspace and a computer room. These spaces are heavily insulated. The exterior of the building will be painted white to minimize solar heating. The dome shell was originally to be white as well, but this was changed as a result of this study.

The thermal model has 21 parts totaling about 2500 elements (see Figure 4). Several simplifying assumptions were made; floors were modeled as equivalent thickness of steel including the building's main beams, columns, joists, girts, deck plates and stiffeners. Some of the model geometry is approximate; for example, the dome slit is not of the correct shape, but it correctly approximates the slit area. The model includes three lumped capacitances to represent the telescope structure, the structural steel of the dome, and the primary mirror. Each capacitance has an associated surface area for convective heat transfer. For the primary mirror, heat transfers from the front surface; the back face was assumed to be effectively insulated. Table 1 summarizes the model material parameters.

Insolation, radiation to the night sky, air leakage (advection) between the internal spaces and the ambient, free and fan-forced ventilation, internal heat generation are all modeled. Relative humidity (a factor in determining the effective night sky temperature) was modeled as varying linearly between 70% at 06:00 to 39% at 18:00, consistent with the statistical average for Flagstaff. The 15 C diurnal air temperature variation typical for late March was modeled using three linear gradients; +1.875 C/hr from 07:00 to 15:00; -1.5 C/hr from 15:00 to 23:00; and -0.375 C/hr from 23:00 to 07:00. Two wind speeds were modeled, 4.76 m/s (the average at the site), and 2.1 m/s, the 20th percentile condition. Winds were considered to be steady.

Table 1. Model material parameters.

Part	Part Name	Component	Material	Surface Condition	Thickness
1	Inside walls	Front Layer	Gypsum	Surface - Paint, White	16 mm
1	Inside walls	Layer 2	Glass, Wool		160 mm
1	Inside walls	Back Layer	Gypsum	Surface - Paint, White	16 mm
2	Chamber floor	Front Layer	Steel (mild)	Surface - Paint, Green	10 mm
2	Chamber floor	Back Layer		Surface - Paint, Green	10 mm
3	Mezzanine floor	Front Layer	Steel (mild)	Surface - Paint, Green	6 mm
3	Mezzanine floor	Layer 2	Glass, Wool		267 mm
3	Mezzanine floor	Layer 3		Surface - Paint, White	500 mm
3	Mezzanine floor	Back Layer	Polyurethane foam	Surface - Paint, White	25 mm
4	Concrete floor	Front Layer	Concrete	Surface - Paint, Green	152 mm
4	Concrete floor	Back Layer		Surface - Concrete, Rough	152 mm
5	Insulated section of pier	Front Layer	Gypsum	Surface - Paint, White	16 mm
5	Insulated section of pier	Layer 2	Glass, Wool		160 mm
5	Insulated section of pier	Back Layer	Concrete	Surface - Concrete	520 mm
6	Chamber air		Standard Air		
6	Chamber air	Advection Link 1			
7	Control room air				
8	Warm concrete floor	Front Layer	Concrete	Surface - Paint, Green	152 mm
8	Warm concrete floor	Back Layer		Surface - Concrete	152 mm
9	Mezzanine air		Standard Air		
9	Mezzanine air	Advection Link 1			
10	R30 ring wall	Front Layer	Steel (mild)	Surface - Paint, White Zinc Oxide	0.6 mm
10	R30 ring wall	Layer 2	Glass, Wool		320 mm
10	R30 ring wall	Back Layer	Gypsum	Surface - Paint, White	16 mm
11	Mezzanine vents	Front Layer	Steel (mild)	Surface - Paint, White Zinc Oxide	1.5 mm
11	Mezzanine vents	Layer 2	Polyurethane foam		19 mm
11	Mezzanine vents	Back Layer	Steel (mild)	Surface - Paint, White	1.5 mm
12	Dome steel		Steel (mild)		
13	Telescope mass		Steel (mild)		
14	R19 ring wall	Front Layer	Steel (mild)	Surface - Paint, White Zinc Oxide	0.6 mm
14	R19 ring wall	Layer 2	Glass, Wool		160 mm
14	R19 ring wall	Back Layer	Gypsum	Surface - Paint, White	16 mm
15	Dome skin	Front Layer	Steel, Mild	Surface - Paint, White Zinc Oxide	0.75 mm
15	Dome skin	Layer 2	Polyurethane foam		100 mm
15	Dome skin	Back Layer	Steel (mild)	Surface - Paint, White	0.6 mm
16	Chamber vents	Front Layer	Steel (mild)	Surface - Paint, White Zinc Oxide	0.7 mm
16	Chamber vents	Layer 2	Polyurethane foam		19 mm
16	Chamber vents	Back Layer	Steel (mild)	Surface - Paint, White	0.6 mm
17	Slit	Front Layer	Steel, Mild	Surface - Paint, White Zinc Oxide	0.75 mm
17	Slit	Layer 2	Polyurethane foam		100 mm
17	Slit	Back Layer	Steel (mild)	Surface - Paint, White	0.6 mm
18	primary mirror		ULE		
19	Lower ring wall	Front Layer	Steel (mild)	Surface - Paint, White Zinc Oxide	0.75 mm
19	Lower ring wall	Layer 2	Glass, Wool		160 mm
19	Lower ring wall	Back Layer	Gypsum	Surface - Paint, White	19 mm
20	Mezzanine pier section	Front Layer	Gypsum	Surface - Paint, White	19 mm
20	Mezzanine pier section	Layer 2	Glass, Wool		160 mm
20	Mezzanine pier section	Back Layer	Concrete	Surface - Concrete	520 mm
21	Roll up door	Front Layer	Steel (mild)	Surface - Paint, White Zinc Oxide	0.6 mm
21	Roll up door	Layer 2	Polyurethane foam		19 mm
21	Roll up door	Back Layer	Steel, Mild	Surface - Paint, White	0.45 mm

The model includes three air nodes; one for the observing chamber, one for the mezzanine level, and a third for the interior warm spaces. Advection between ambient air and the chamber and mezzanine air nodes varied as a function of time to simulate opening the chamber and mezzanine vents at night from 18:00 to 07:00. With the vents closed air flow was reduced to a nominal leak rate of one chamber volume per hour. The air velocity over the primary mirror surface was set to 13% of the free-stream wind speed, consistent with the results of the CFD study.

5. Model results

Figure 5 shows the exterior of the model at 2 hour intervals over a 24 hour period. Sunset is at the upper left. Over the course of the evening the dome shell cools by radiation to the cold sky until it is balanced by convective heat gain from the ambient air. Insolation is clearly visible as the sun illuminates portions of the dome shell.

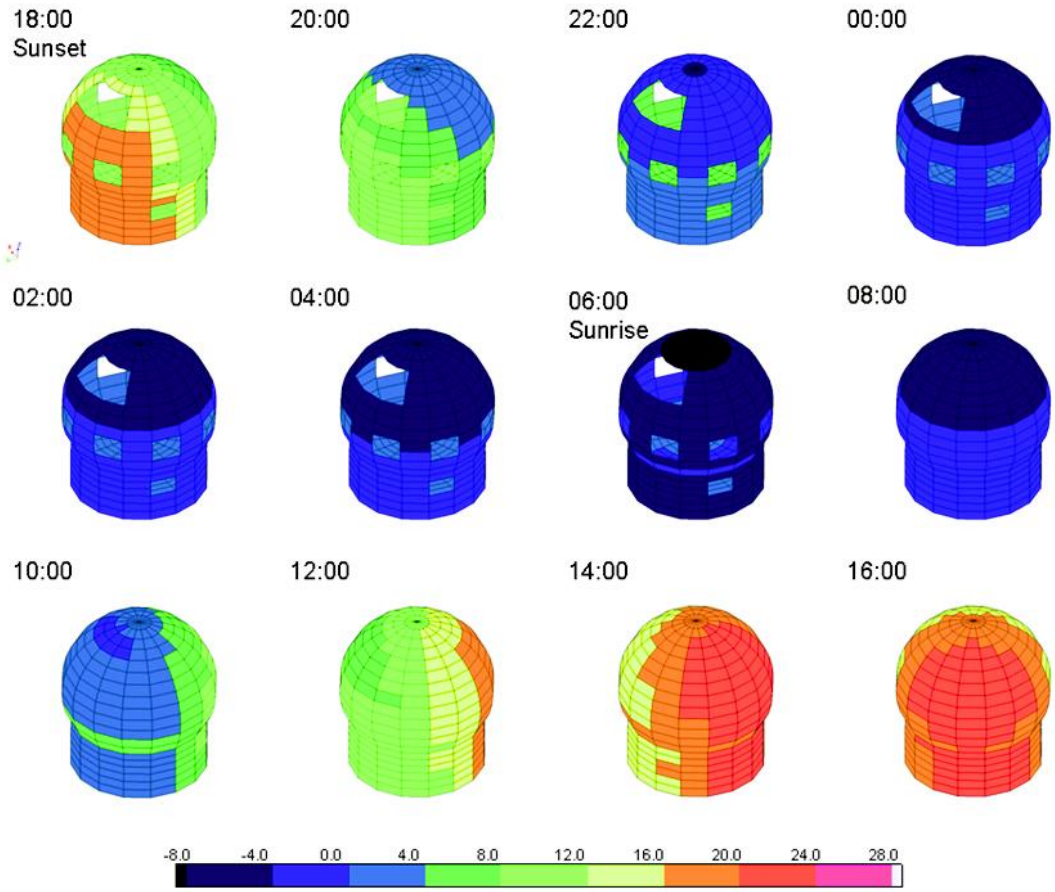

Figure 5. Transient thermal model over a 24 hour period from sunset at 18:00 hours at upper left. Progressive cooling due to radiation to the night sky can be seen from 22:00 to 08:00; the track of the sun can be discerned as it advances over the dome surface from 10:00 to 18:00.

The model was run to generate transient temperature histories for the dome shell, chamber air, and primary mirror; these are shown in Figure 6. It appears that the facility performs generally as intended; soon after opening the vents, the air in the chamber converges to within a fraction of a degree of the ambient air temperature; with the vents and slit closed the temperatures gradually increase though the day until opening when they again rapidly equilibrate. Steel structures tend to lag behind the chamber air temperature due to thermal inertia; as the chamber temperature decreases the structures give up their stored heat. Similarly, the temperature of the primary mirror lags behind the changing chamber air temperature due to its thermal inertia.

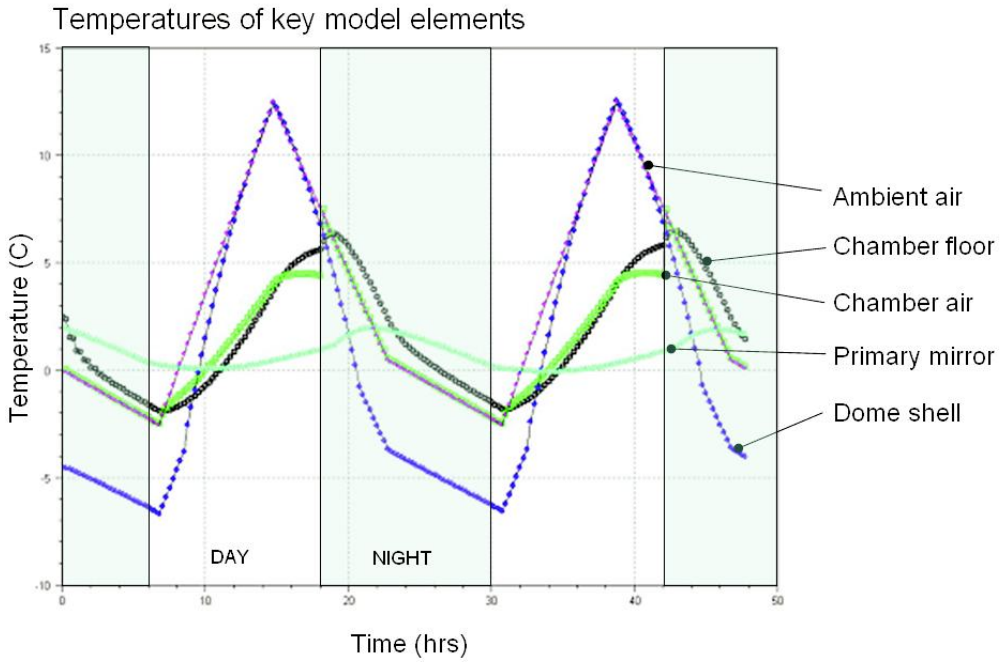

Figure 6. Time history plot of the key elements over a 48 hour period starting at midnight. The white painted dome shell cools about 5C below ambient by radiation to the night sky. The primary mirror temperature lags behind the chamber air temperature due to thermal inertia. These data were used to generate the seeing estimates in Figure 7.

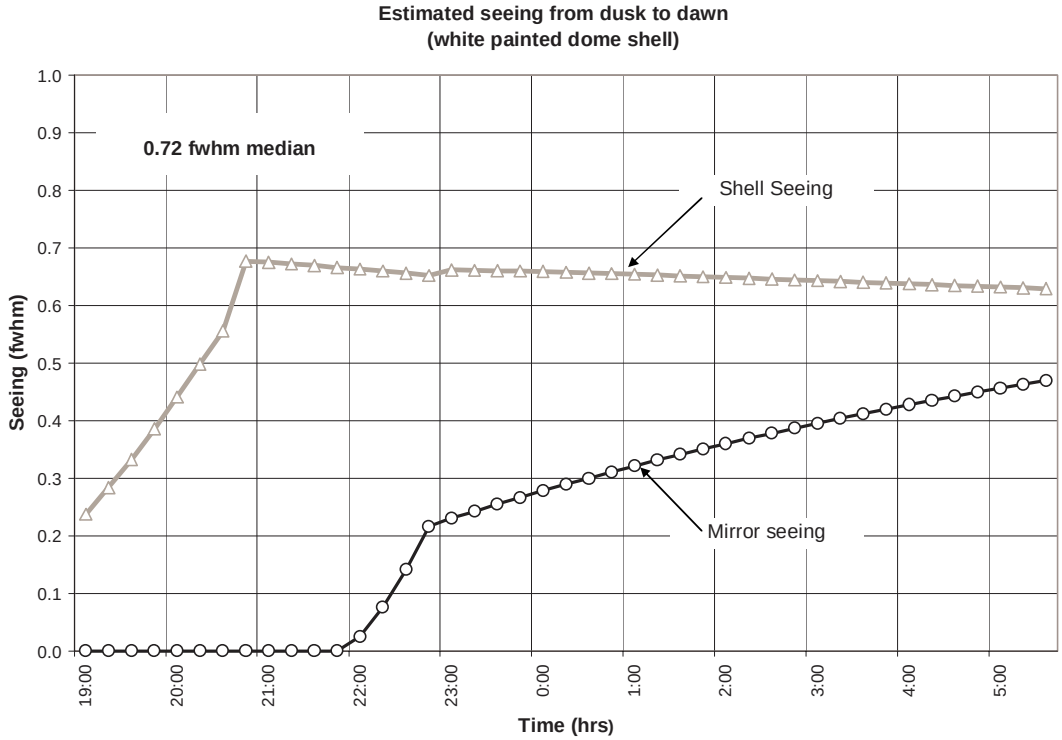

Figure 7. Night time seeing estimates based on the temperature data in Figure 6. The white painted dome shell rapidly cools by radiation to the night sky until it reaches an equilibrium balanced by convection. Consequently shell seeing rapidly increases to a plateau. Mirror seeing starts when the chamber air temperature falls below the primary mirror and increases through the night.

6. Seeing estimates

The data in Figure 6 were used to estimate instantaneous facility seeing shown in Figure 7. The model predicts that seeing will be best early in the evening when key temperatures are closest to equilibrium with the ambient air temperature. At the start of the night the primary mirror is cooler than ambient air and does not contribute to seeing. By 22:00 the chamber air temperature drops below the primary mirror temperature and mirror seeing starts to build, increasing through the remainder of the night. Radiation to the night sky cools the dome shell to below ambient air temperature introducing shell seeing. The model indicates that the local seeing will deteriorate through the night reaching about 0.8 fwhm by dawn. Models were run at two wind speeds, the median 4.76 m/s and the 20% percentile 2.1 m/s wind speeds; the lower wind speed over the mirror surface results in greater mirror seeing. Surprisingly, the difference in wind speed has very little effect on the shell seeing. The median seeing degrades from 0.72 fwhm at 4.76 m/s to 0.81 fwhm at 2.1 m/s wind speeds.

7. Mitigating shell seeing

The estimated 0.72 to 0.81 fwhm local seeing for the nominal facility was not considered acceptable. Fortunately there are several cost effective measures that can be implemented to reduce seeing. In recent years many older observatories, and some newer ones, have retrofitted their facilities with dramatic improvement in seeing. It is always better to build features into the facility rather than retrofit.

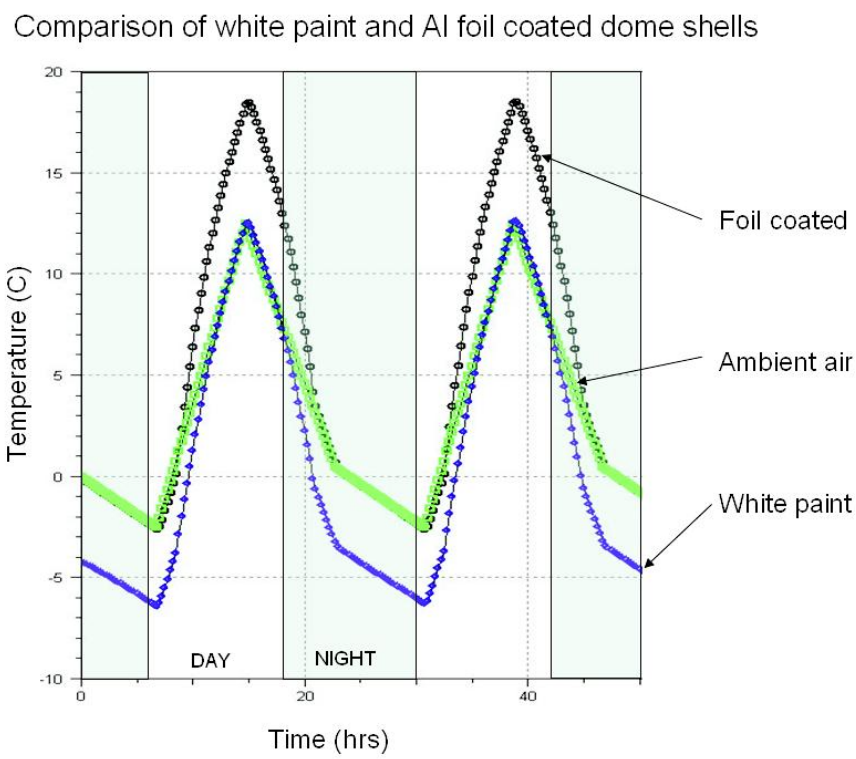

Figure 8. When coated with white paint a dome shell stays closer to ambient air temperature during the day but cools below ambient at night; the aluminum foil-coated shell overheats during the day, but stays closer to ambient temperature at night.

Several observatories have coated their domes with adhesive backed aluminum foil tape such as 3M product #425. This reflective material has low emissivity and reasonably low absorptivity (0.05 and 0.2 respectively for fresh tape). This greatly reduces radiation to the sky. Compared to the typical observatory white paint, the overall solar gain is reduced, but with the reduced emissivity, the radiative losses are also reduced so there is a net increase in heat gain during the

day. At night an aluminum coated dome stabilizes at close to ambient air temperature, while a white dome typically cools to about 5 C below ambient. Accumulated dust can diminish the effectiveness by about 20%.

The model was run simulating the application of aluminum foil tape; Figure 8 compares the shell temperature history for the foil coated and white-painted domes. The white painted dome stays close to ambient air temperature during the day, while the foil coated dome stays close to ambient air temperature during the night; consequently ***solar observatories should be white, night-time observatories should be silver.***

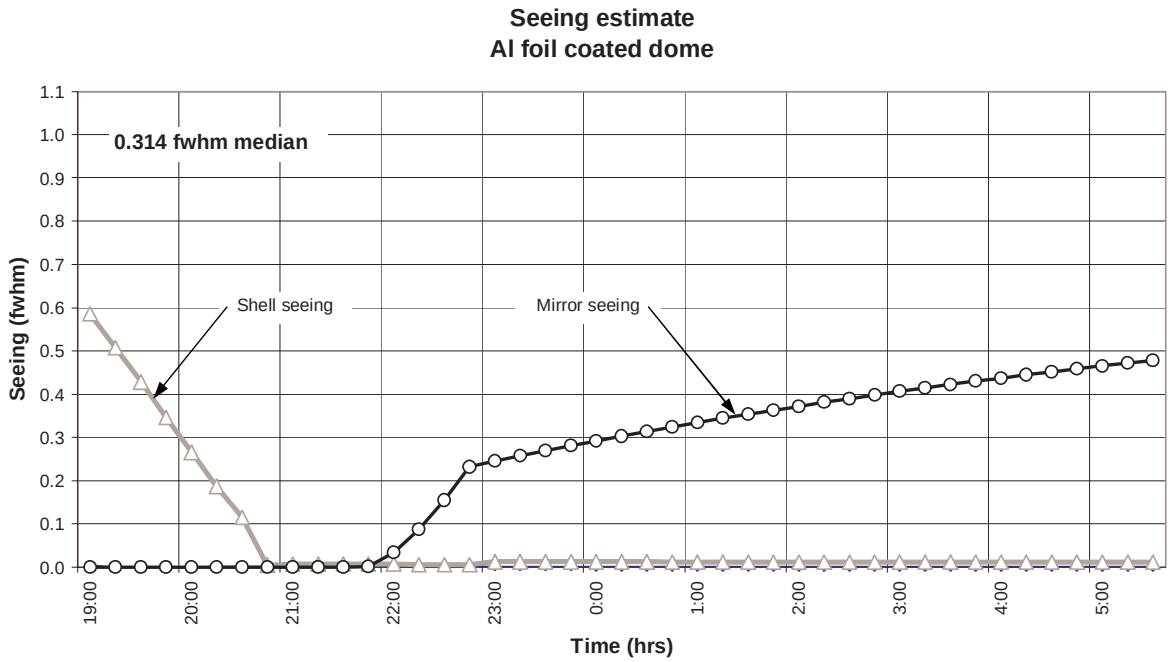

Figure 9. Coating the dome shell with self adhesive aluminum foil tape (3M #425) reduces shell seeing to near zero by 21:00. After 22:00 mirror seeing begins and increases through the remainder of the night.

Seeing estimates for the foil coated dome are shown in Figure 9. Due to the increased daytime heat gain the dome shell is still warm at the start of the night introducing shell seeing. This decreases as the dome shell cools to ambient temperature; by about 21:00 the shell seeing has virtually disappeared. As we saw in Figure 7, the decreasing air temperature dips below the primary mirror temperature at around 22:00 and mirror seeing grows through the remainder of the night. Median seeing through the night is reduced to 0.31 arcsec fwhm at 4.76 m/s wind speed, or 0.52 fwhm at 2.1 m/s winds and is mostly due to mirror seeing. The model indicates the best seeing will occur about three to four hours after opening.

8. Mitigating mirror seeing

Examination of Zago's expressions (equations 3 to 5) suggests two strategies that could be used for reducing mirror seeing; by controlling the mirror temperature or by controlling the flow of air over the primary mirror surface. The technique has been demonstrated in laboratory experiments but is relatively untried in real observatory conditions. For best results the air flowing over the primary be at the ambient air temperature and should be dry, implying an infrastructure capable of supplying a continuous flow of pressurized, temperature-controlled, dehumidified air. An air flow system was partially implemented for the SOAR telescope but has not been activated; other air flow systems at AEOS and UKIRT are not being used. By contrast, control of the mirror temperature is being done at many observatories and has proven effective in reducing mirror seeing.

With the primary mirror represented by a single-node "lumped capacitance" the present model is too coarse to use for the design of a mirror cooling system. However, as a demonstration of the potential, the model was run introducing constant heat extraction from the primary mirror node. The resulting temperature history is shown in Figure 10. A continuous 24-hour extraction of 135 W was sufficient to lower the temperature of the primary mirror to below ambient for most of the night reducing the mirror seeing contribution to near zero. A practical system would likely be sized to two or three times this capacity, sufficient to drive the mirror temperature to follow day to day weather changes.

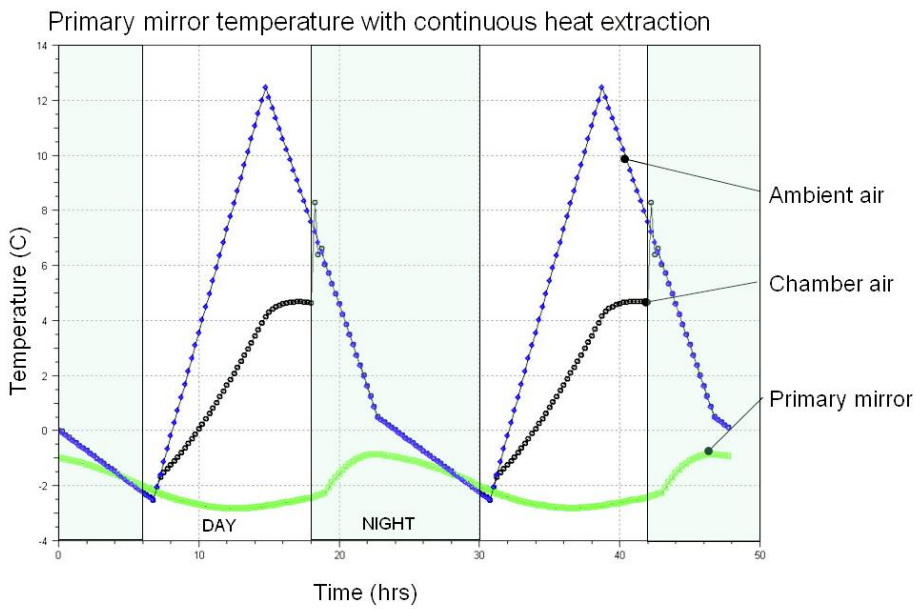

Figure 10. Extracting heat from the primary mirror can reduce its temperature and so reduce mirror seeing. Here a modest but continuous (24-hr) extraction rate of 135 W from the back of the mirror has been modeled.

9. Residual sources of seeing

Implementing the mitigating strategies suggested in the preceding two sections is likely to significantly reduce the local seeing to the point where other lesser sources limit the local seeing. We previously noted that the steel floor of the observing chamber lags behind the chamber air by up to 2 C and could be a significant source of seeing. This can be reduced by insulating the floor with a layer of polyurethane foam batting and plywood deck over the existing steel plate.

Contributions from other sources estimated in the Delivered Image Quality Budget [2007] include 0.058 fwhm from chamber interior surfaces and 0.069 fwhm from either the secondary mirror or prime focus corrector. Adding these in quadrature gives an estimate of 0.09 fwhm from these sources.

10. Conclusion

As with atmospheric seeing, local seeing is a statistical quantity. Over the past ~three decades there has been a great deal of progress in standardizing and collecting seeing measurements, identifying correlations with local environments and developing expressions that quantify the statistical mean. Three major sources have been identified; mirror seeing, shell seeing and dome seeing. These are driven by temperature differences between key surfaces and air volumes: between the ambient and the exterior of the shell; between ambient and the chamber air; and between the chamber air and the primary mirror surface. These contributors can be discerned by examining schlerien images. Other sources of seeing should not be neglected, but are usually minor in comparison.

A thermal modeling program such as WinTherm® is an effective tool for predicting the key temperatures; formulae can be used to predict the average local seeing. A fairly simple thermal model can provide insight into the dynamic behavior of the local observatory environment, and is useful for evaluating various options and strategies.

Several cost effective strategies work quite well to control local seeing; sealing and insulating warm spaces, passively ventilating the chamber, use of lightweight, low thermal inertia construction for structures, insulating the shell against daytime heat gain, and choosing exterior coatings with desirable properties. The best coatings currently available are white paint for solar observatories and aluminum foil nighttime observatories. Active thermal control is the least cost effective measure and should be used when there are no better options. The primary mirror is perhaps the most troublesome source of seeing; due to its thermal inertia, the mirror is rarely in equilibrium with the surrounding air. Controlling air flow over the primary works in principle, but it is not practical; active cooling is the appropriate choice.

An observatory operates in a dynamic thermal equilibrium; the temperatures of key surfaces and air volumes cycle diurnally with an amplitude and phase lag determined by their thermal inertia and coupling. Even a poorly designed facility may have periods of excellent seeing when key temperatures converge, much like a broken clock that is perfectly accurate twice a day. In a more typical scenario, local seeing may cross through a minimum then deteriorate through the course of the night as temperatures diverge. With simple, cost effective strategies, a well designed facility will can suppress local seeing throughout the night.

References

[1] N. Dalrymple, J. Oschmann, Jr., and R. Hubbard, “ATST enclosure: seeing performance, thermal modeling, and error budgets”, Proc. SPIE Volume 5497, 497 (2004).
[2] N. Dalrymple, “Mirror seeing”, ATST Project Documentation RPT-0003 (2003).
[3] R. Ford, “Seeing control strategy for the Gemini 8m enclosure”, GEMINI Project Report RPT-TE-G0039 (1993).
[4] R. Racine, D. Salmon, D. Cowley, and J. Sovka, “Mirror, dome and natural seeing at CFHT,” Pub. Astron. Soc. Pacific 103, pp. 1020–1032 (1991).
[5] L. Zago, “The Effect of Local Atmospheric Environment on Astronomical Observations,” Thesis No 1394 (1995) Ecole Polytechnique Federale de Lausanne (1995).
[6] D. Blanco, C. Corson, and D. Sawyer, “Seeing Experiments with the WIYN 3.5 meter Telescope,” Proc. SPIE Volume 4004 (2000).
[7] “DCT – CFD Ventilation Report”, DCT -0140A-001-1, by Thermodynamics, Fluids & Design (TFD), 2003.
[8] “Happy Jack Site Environment”, DCT 0800a-001-1 (2004).
[9] J.Terán, T. Sebring, D.Neff, M. de Kock, “Design of the Discovery Channel Telescope Enclosure”, Proc. SPIE Volume 5489 (2003).
[10] D. Blanco and M. Johns, “Thermal design of the WIYN 3.5-meter telescope enclosure”, Proc. SPIE Volume 2199 (1994).
[11] “Delivered Image Quality Budget”, DCT-0810A-001-B (2007).